Received: 13 August 2022 | Revised: 27 October 2022 | Accepted: 6 November 2022

DOI: 10.1002/aic.17960

AIChE JOURNAL

RESEARCH ARTICLE

Reaction Engineering, Kinetics and Catalysis

An experimental and theoretical study on the effects of amine chain length on CO_2 absorption performance

Ding Wei | Qinlan Luo | Tong Ouyang | Qie Liu | Yangqiang Huang | Bo Jin | Hongxia Gao | Xiao Luo | Zhiwu Liang

College of Chemistry and Chemical Engineering, Hunan University, Changsha, People's Republic of China

Correspondence
Xiao Luo and Zhiwu Liang, College of Chemistry and Chemical Engineering, Hunan University, Changsha 410082, People's Republic of China.
Email: x_luo@hnu.edu.cn and zwliang@hnu.edu.cn

Funding information
National Natural Science Foundation of China, Grant/Award Number: 22178089

Abstract

To explore the effect of amine chain length on CO_2 absorption performance, the reaction kinetics of CO_2 absorption in aqueous 1-dimethylamino-2-propanol (DMA2P), 1-diethylamino-2-propanol (DEA2P), 2-(methylamino)ethanol (MAE), and 2-(ethylamino)ethanol (EAE) solutions with different concentrations were explored using the stopped-flow apparatus. Additionally, Density Functional Theory (DFT) calculations were conducted to examine the reaction mechanism and the free energy barrier of the elementary reactions underlying CO_2 absorption in these four aqueous amine solutions. Kinetic models for CO_2 absorption in tertiary amines and secondary amines were established, based on the base-catalyzed hydration mechanism and the zwitterion mechanism, respectively, both of which perform well in predicting the relationship between k_0 and the amine concentration. The free energy barrier obtained by DFT is consistent with the activation energy barrier trend obtained by experiment. In addition, the effect of chain length on the free energy barrier was investigated through the chemical bond and weak interaction analysis.

KEYWORDS
CO_2 capture, DFT calculation, reaction kinetics, reaction mechanism, stopped-flow

1 | INTRODUCTION

With the increase of carbon dioxide (CO_2) emissions to the atmosphere, the greenhouse effect and climate change are becoming more serious.[1,2] Among greenhouse gas and climate change amelioration options, CO_2 capture and storage (CCS) is widely seen as having the potential to solve these problems.[3] Capturing CO_2 is the first step in CCS and accounts for 70%–80% of the total cost of this technology. There are three basic types of CO_2 capture: precombustion CO_2 capture, oxy-fuel combustion, and postcombustion CO_2 capture (PCC). In PCC, the fossil fuel is burnt as in conventional energy generation and the CO_2 is extracted from the combustion effluent gas. Therefore, PCC technology can be retrofitted to existing CO_2 emission sources, such as coal-fired power stations,[4] making it the most widely studied and used large-scale CO_2 capture method. In addition, PCC is seen as the most economical, practical approach to reducing CO_2 emissions in the short to medium term.[5]

Among the various PCC technologies, chemical absorption (e.g., using aqueous amine solutions), is the most mature postcombustion carbon capture technology.[6] Amine scrubbing was used at a small scale in early 1980,[7] and it has been utilized in two commercial-scale postcombustion capture facilities in coal-fired power plants (Boundary Dam[8,9] and Petra Nova[3]). Researchers consider chemical absorption of CO_2 by alkane amine solutions as the most economical and efficient technology for capturing CO_2 from fuel-fired power plants.[10]

Common amines can be divided into primary amine, secondary amine, and tertiary amine groups. Among them, the most commonly studied amine absorbent is monoethanolamine (MEA),[11–14] which is

Ding Wei and Qinlan Luo contributed equally to this work.

also the most widely used primary amine in industry.[15] In addition, there have also been many studies of mass transfer performance, reaction kinetics and energy consumption during absorption and desorption by other primary,[16] secondary,[17] and tertiary[18–20] amines and amino acid salts[21] in aqueous solution.

Compared with traditional primary amines, secondary amines possess a moderate absorption rate, absorption capacity, heat of reaction, and enhanced chemical stability, and can be used to replace MEA.[22–24] Tertiary amines have a different reaction mechanism from primary and secondary amines. They have a slow reaction rate with CO_2 during absorption but require less energy for CO_2 desorption, a characteristic that makes them potentially useful in large scale processes for the absorption of CO_2.[25,26]

The absorption and desorption performance of amines is strongly related to the amine molecular structure.[26] One variable, the amine chain length, has a significant effect on the absorption of CO_2 by aqueous amine solutions. For further progress in the development and improvement of amine absorbents, it is necessary to understand the effect of the chain length of the amines and the corresponding reaction mechanisms underlying the absorption of CO_2.

At present, most studies only focus on the effect of amine chain length on absorption or desorption performance of aqueous amine solutions through experimentation, but the elementary reaction mechanism is still unclear. Some studies using the stopped-flow technique indicate that the reaction rate of some commonly used tertiary amines with long alkyl chains is faster than that of amines with short alkyl chains.[26,27] In addition, our previous studies[19] have observed that the side carbon chain promotes the activity of commercial tertiary amines. However, the fundamental mechanism behind the effect of chain length has not been investigated because of the difficulty of exploring the nature of the free energy barrier in the experimental process. Therefore, it is necessary to study the effect of the chain length of the amine and the corresponding reaction mechanism underlying the CO_2 absorption by amine solutions through theoretical computational model methods.

There have been many studies that have obtained the values of reaction energy barriers through theoretical calculations, but there are fewer theoretical calculations to explain the nature of energy barriers. Therefore, it is crucial to find a suitable analytical method to explain the energy barrier. Wolters et al.[28] and Bickelhaupt et al.[29] both proposed the activation strain model to analyze the energy barrier. In addition, Bader et al.[30] proposed the theory of atoms in molecules (AIM) and defined van der Waals (vdW) surfaces by 0.001 density isosurface,[31] which allowed the vdW interaction to be represented. Astakhov et al.[32] revealed the features of the charge-shift bond and noncovalent molecular interactions by combining the information-theoretical description of electron density with density functional theory (DFT). Lipkowski and Grabowski et al.[33] proved the existence of dihydrogen bonds according to the topological analysis based on the Bader theory. These provide us with ideas to study the nature of the free energy barrier by chemical bond and weak interaction analysis. So, the study of reaction mechanism and kinetics from DFT calculations combined with experimental validation is instructive for the development of aqueous amine solutions and provides for a better explanation of their nature.

2-(Methylamino)ethanol (MAE), a secondary amine, will remain competitive in the future due to its effective desorption and fast absorption kinetics.[24] 1-dimethylamino-2-propanol (DMA2P) exhibits good behavior not only in CO_2 absorption capacity and CO_2 absorption heat, but also in CO_2 absorption rate, reaction kinetics and relatively better mass transfer performance than methyldiethanolamine (MDEA).[34] Therefore, two secondary amines (MAE and 2-(ethylamino) ethanol [EAE]) and two tertiary amines (DMA2P and 1-diethylamino-2-propanol [DEA2P]) have been selected for this study.

In the present study, the effects of different chain lengths of secondary and tertiary amines on CO_2 absorption in aqueous solutions have been fully explored. In addition, the reaction mechanism of CO_2 absorption in aqueous secondary and tertiary amines solutions has also been studied experimentally and theoretically. The stopped-flow apparatus was implemented to analyze the reaction kinetics and explore the reaction model of CO_2 reacting with those aqueous amine solutions. The DFT calculations have also been conducted to examine the effect of aqueous amine solutions with different chain lengths on the mechanism and kinetics of CO_2 capture, as compared to the experimental results. As well, the effect of chain length on the free energy barrier has been studied by combining the activated strain model with chemical bond and weak interaction analysis.

2 | EXPERIMENTS AND CALCULATIONS

2.1 | Experimental section

2.1.1 | Chemicals

Figure 1 shows the chemical molecular structures of MAE, EAE, DMA2P, and DEA2P. MAE (purity 99%) and EAE (purity 99%) were purchased from Shanghai Aladdin Biochemical Technology Co., Ltd., DMA2P (purity 98%) was purchased from Aladdin Industrial Corporation., and DEA2P (purity 98%) was purchased from TCI, Japan. All amines in this work were not subjected to further purification. CO_2 (purity 99%) was provided by Changsha Jingxiang Gas Co., Ltd. The deionized water was provided by a deionized water unit manufactured by TaoShi Water Equipment Engineering Co., Ltd., China.

2.1.2 | Stopped-flow apparatus

The chemical reaction rates between CO_2 and aqueous amine solutions can be measured using the stopped-flow apparatus, model SF-61DX manufactured by Hi-Tech Scientific, Ltd. (UK). As presented in Figure 2, the stopped-flow apparatus includes four major sections, and the temperature is controlled within ±0.1 K by circulating water. The change in conductivity caused by ion formation in the reaction system is measured by a conductivity detection cell[35] and provides an intuitive reaction rate. Pertinent details can be found in previous

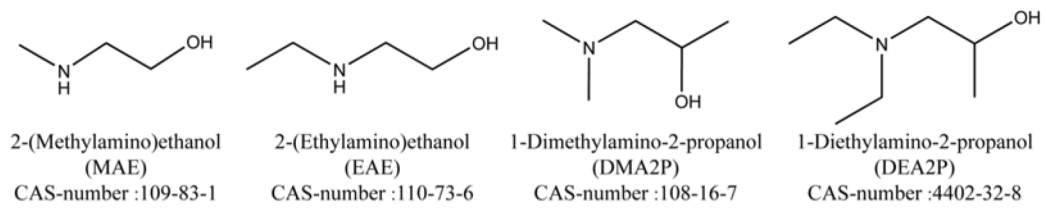

FIGURE 1 Chemical structures of MAE, EAE, DMA2P, and DEA2P.

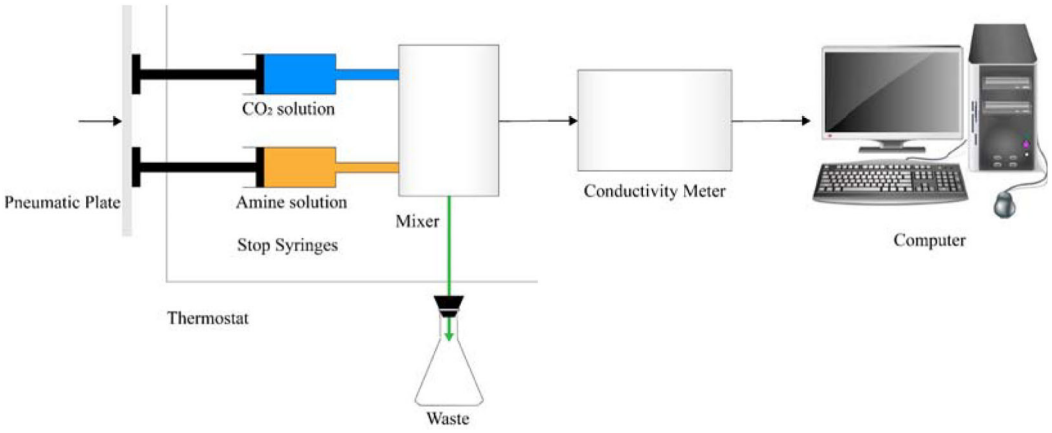

FIGURE 2 The schematic drawing of the stopped-flow apparatus.

studies.[36–39] The curve of conductivity vs. time is then fitted in the microprocessor, and the fitting equation is given in the form:

$$Y = -A \cdot \exp(-k_0 \cdot t) + C \quad (1)$$

The fitted parameter k_0 represents the observed pseudo first-order reaction rate constant. It can be automatically obtained by the Kinetasyst software which is the operational software of the stopped-flow apparatus.

2.1.3 | Experimental procedure

The stopped-flow technique is based on detecting the variation in electric conductivity in the solutions, and can only collect valid data under low amine concentrations due to the otherwise too large changes of conductivity. Therefore, the concentration of amine usually is set to be less than 1 kmol/m^3 for tertiary amines, and less than 0.1 kmol/m^3 for primary or secondary amines. The specific concentration range chosen needs to be determined by preliminary experiments. In this work, concentrations of MAE and EAE between 0.02 and 0.03 kmol/m^3, and concentrations of DMA2P and DEA2P between 0.1 and 0.2 kmol/m^3 were found to be appropriate to test the concentration effects on reaction rate.

The CO_2 saturated aqueous solutions were prepared by bubbling CO_2 into deionized water in a glass gas washing bottle for at least half an hour. Then, the CO_2 aqueous solution used for the final experiment was obtained by diluting the CO_2 saturated aqueous solution 10 times. In the amine solutions, the total concentration of amine is more than 10 times higher than that of the CO_2 to ensure that the reaction occurs under pseudo first-order conditions. All the experiments were carried out at temperatures of 293, 298, 303, 308, and 313 K in the stopped-flow equipment.

2.2 | Reaction mechanism and kinetics models

2.2.1 | Base-catalyzed hydration mechanism

Donaldson and Nguyen[40] understood that tertiary amines may not interact directly with CO_2, and proposed the following mechanism:

$$R_1R_2R_3N + CO_2 + H_2O \rightleftharpoons R_1R_2R_3NH^+ + HCO_3^- \quad (2)$$

At very high pH, a direct interaction between CO_2 and the tertiary amine is possible to form monoalkyl-carbonate.[41] When pH < 12, this reaction is negligible and the reaction rate r_{CO_2} can be expressed as:

$$r_{CO_2} = k_2[CO_2][R_1R_2R_3N] \quad (3)$$

$$k_0 = k_2[R_1R_2R_3N] \quad (4)$$

In this study, k_0 was measured with the stopped-flow apparatus.

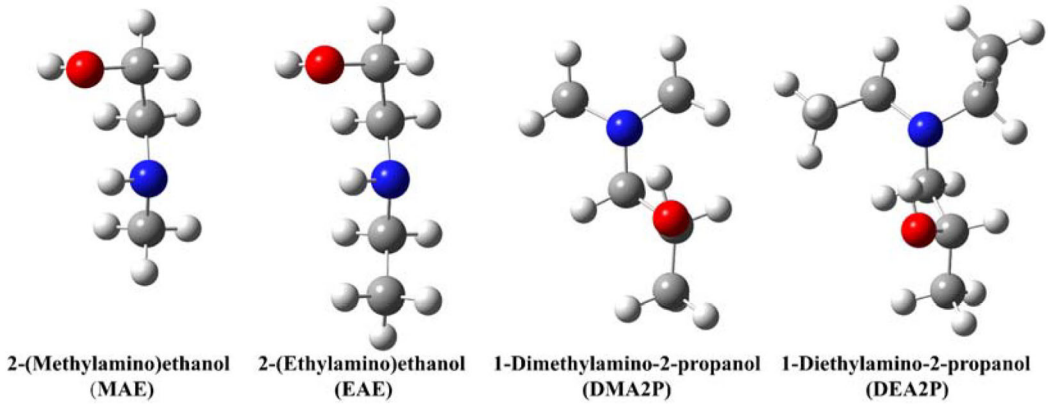

FIGURE 3 Lowest-energy geometric structures of MAE, EAE, DMA2P, and DEA2P.

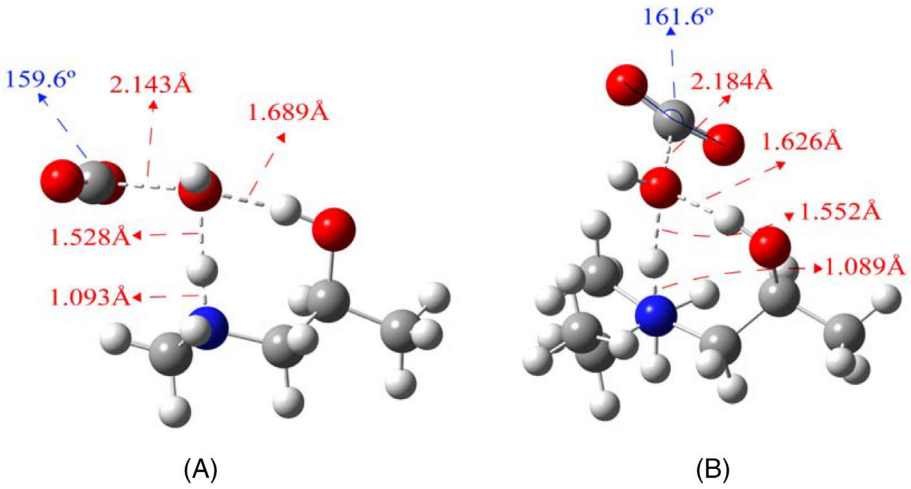

FIGURE 4 CO_2 and H_2O reaction with tertiary amine: (A) The TS calculation structure of DMA2P; (B) The TS calculation structure of DEA2P. The red number is the bond length, the blue number is the bond angle.

2.2.2 | Zwitterion mechanism

The zwitterion mechanism was suggested by Caplow[42]; and is based on having the whole reaction process divided into two reaction steps:

$$CO_2 + R_1R_2NH \underset{k_{-1}}{\overset{k_1}{\rightleftarrows}} R_1R_2NH^+COO^- \text{ (zwitterion formation)} \quad (5)$$

$$R_1R_2NH^+COO^- + B \xrightarrow{k_B} R_1R_2NCOO^- + HB^+ \quad \text{(Deprotonation of zwitterion)} \quad (6)$$

At very low concentrations of CO_2, the concentration of carbamate is so low that Equation (6) can be considered irreversible. Under the steady-state-intermediate conditions, the reaction rate of CO_2 (r_{CO_2}) in aqueous solutions can be expressed as:

$$r_{CO_2} = \frac{k_1[R_1R_2NH]}{1 + \frac{k_{-1}}{\sum k_B[B]}}[CO_2] \quad (7)$$

where k_B represents the rate constant of deprotonation of zwitterion from zwitterion to any proton acceptor in solution, for example, CO_3^{2-}, H_2O,HCO_3^-, OH^-, or R_1R_2NH. When $k_{-1} \gg k_B[B]$, the rate equation of Equation (7) transforms into:

$$r_{CO_2} = \frac{k_1 \sum k_B[B]}{k_{-1}}[R_1R_2NH][CO_2] \quad (8)$$

For amines R_1R_2NH and water, Equation (8) can be extended to:

$$r_{CO_2} = \frac{k_1}{k_{-1}}(k_{amine}[R_1R_2NH] + k_{H_2O}[H_2O])[R_1R_2NH][CO_2] \quad (9)$$

Since k_{amine} and k_{H_2O} cannot be solved separately, $\frac{k_1 k_{amine}}{k_{-1}}$ and $\frac{k_1 k_{H_2O}}{k_{-1}}$ are replaced by the compound rate constants k_3^{amine} and $k_3^{H_2O}$, Equation (9) becomes:

$$r_{CO_2} = \left(k_3^{amine}[R_1R_2NH] + k_3^{H_2O}[H_2O]\right)[R_1R_2NH][CO_2] \quad (10)$$

$$k_0 = \left(k_3^{amine}[R_1R_2NH] + k_3^{H_2O}[H_2O]\right)[R_1R_2NH] \quad (11)$$

In this study, k_0 was measured with the stopped-flow apparatus.

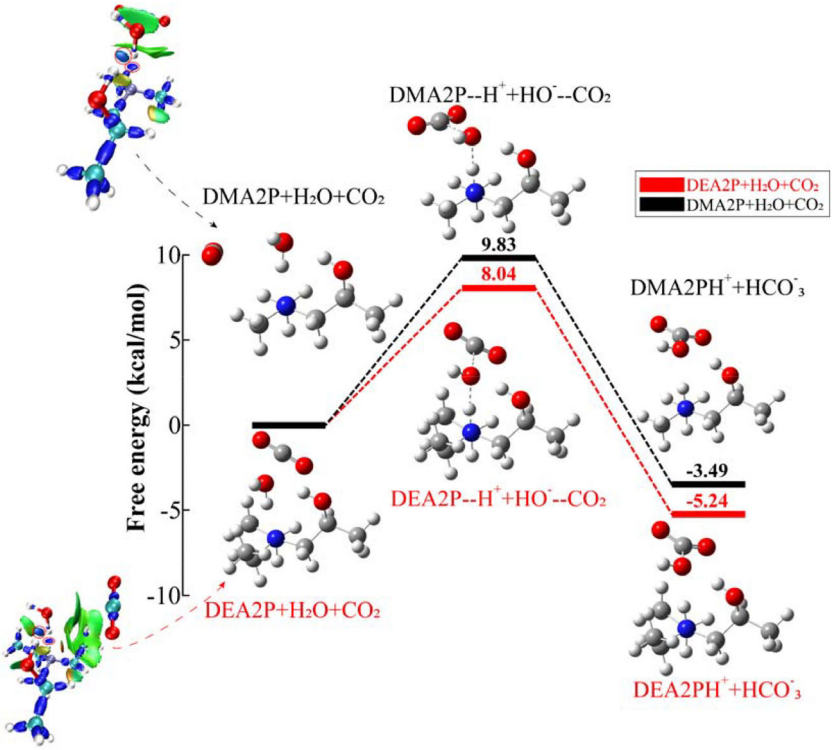

FIGURE 5 Free energy barrier diagram of DEA2P and DMA2P. The calculated temperature and pressure are 298 K and 1 bar.

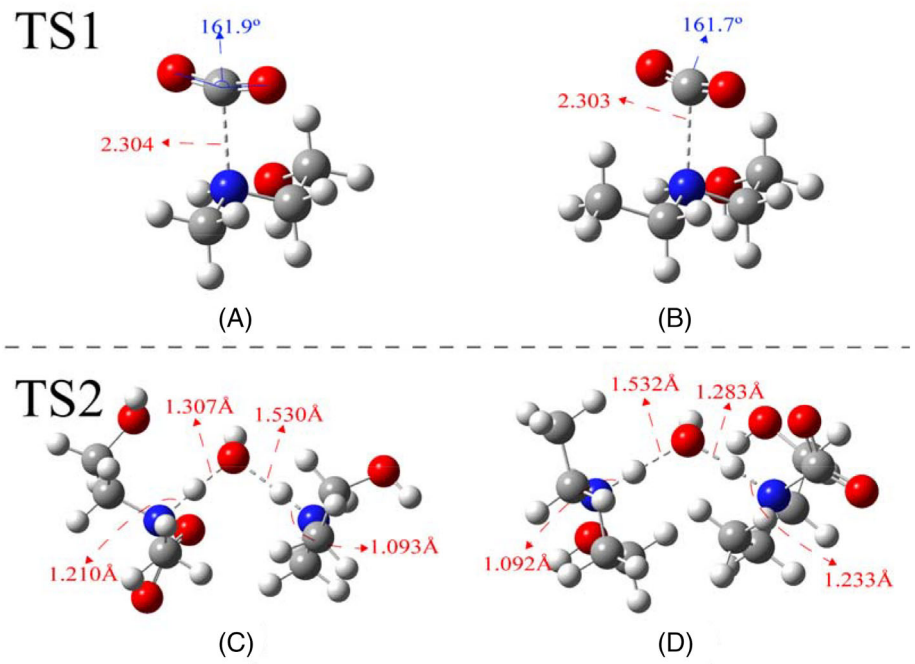

FIGURE 6 CO_2 and H_2O reaction with tertiary amine: (A) The TS1 calculation structure of MAE; (B) The TS1 calculation structure of EAE; (C) The TS2 calculation structure of MAE; (D) The TS2 calculation structure of EAE. The red number is the bond length, the blue number is the bond angle.

2.3 | Calculation section

In this study, the Gaussian 16 software package[43] was used for the DFT[44] calculation. Gaussian 16 was invoked by Molclus Program[45] to search the molecular structures of the above four alkanolamines, with the functional and basis set at B3LYP/6-31G*.[46–50] The keyword "EmpiricalDispersion = GD3BJ"[51] was added because B3LYP functional cannot describe the dispersion interaction. The solvent effects were determined using the universal solvation model (SMD).[52] The energy of various conformations was obtained, the five with the lowest energy were selected, and the basis set def2-TZVPP[53] with higher accuracy was adopted. Then the optimized geometries, harmonic frequencies, and Gibbs free energy of transition states, reactants, and products were obtained at the level of B3LYP/def2TZVPP. All

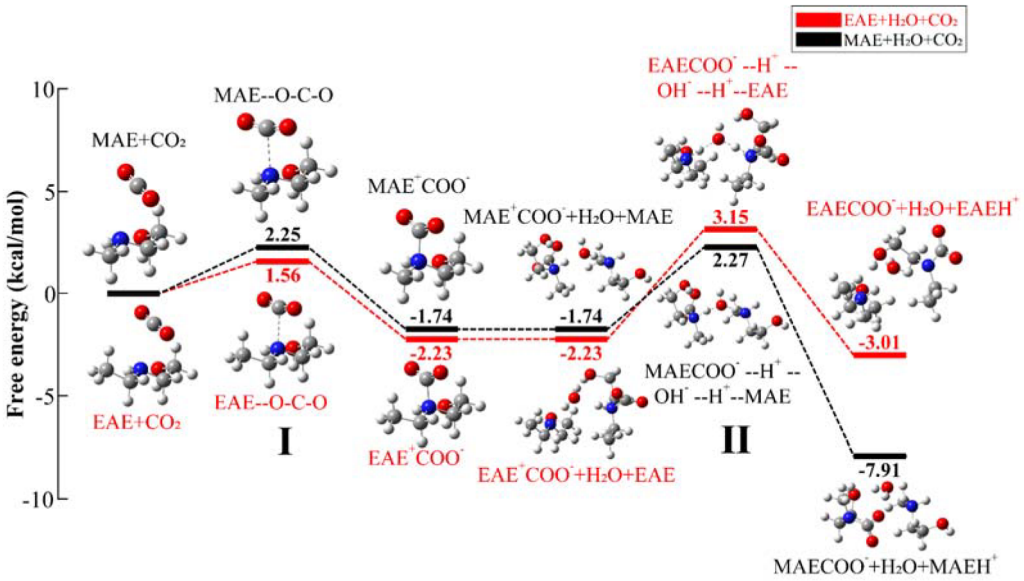

FIGURE 7 Free energy barrier diagram of EAE and MAE. The calculated temperature and pressure are 298 K and 1 bar.

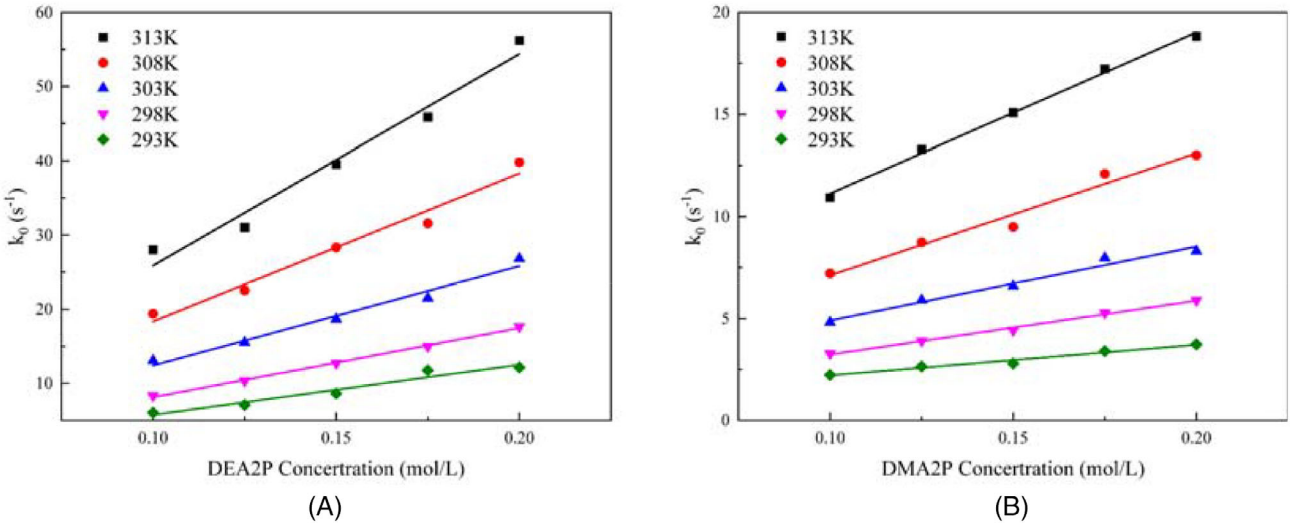

FIGURE 8 The k_0 of DEA2P (A) and DMA2P (B) as function of concentration at different temperatures.

stationary points of the potential energy surface (PES) corresponded to the local minima, all with real vibrational frequencies, or with transition states characterized by only one imaginary frequency. Energy and force were obtained from the intrinsic reaction coordinate (IRC) method.[54] The initial and final states were also obtained from the IRC method. The free energy barrier was obtained from the Gibbs free energy of the optimized transition state and initial state.

To explain the high and low free energy barrier, we used the Multifunctional wavefunction analyzer (Multiwfn 3.8)[55] and Visual Molecular Dynamics (VMD1.9.3)[56] to analyze and visualize the calculated wave function. This included the Interaction Region Indicator (IRI)[57] method to show chemical bonds and weak interactions in chemical systems, and Atoms in Molecules (AIM) to analyze chemical bonds and weak interactions strength.[30,58]

3 | RESULTS AND DISCUSSION

3.1 | Calculation results

Since the structure of the amine molecule has a great influence on the subsequent calculation, the determination of the initial structure of the amine molecule becomes particularly important. Therefore, the gentor component of Molclus Program was used to search for the molecular structures of the four amines. After that, Gaussian 16 was invoked through the Molclus Program to calculate energy. Five structures with the lowest energy were selected. Then B3LYP/def2TZVPP with higher precision was selected for the calculation to determine which structure has the lowest energy. The lowest-energy geometric structures of MAE, EAE, DMA2P, and DEA2P are shown in Figure 3.

TABLE 1 CO_2-DMA2P(DEA2P)-water system second-order reaction rate constants at different temperatures

Temperatures (K)	k_2^{DMA2P}	k_2^{DEA2P}
293	19.44 ± 0.60	60.39 ± 1.93
298	30.21 ± 0.50	84.79 ± 1.03
303	45.56 ± 1.17	124.57 ± 2.46
308	69.15 ± 1.45	188.95 ± 4.03
313	100.54 ± 2.48	263.66 ± 5.78

3.1.1 | Reaction mechanism and free energy barrier calculation of CO_2 absorption in aqueous tertiary amine solutions

Based on the base-catalyzed hydration mechanism for the reaction between a tertiary amine and CO_2, the Gibbs free energies of the initial state, transition state and final state were calculated by Gaussian16. First, we obtained the TS structures as shown in Figure 4. When CO_2 and H_2O begin to react with a tertiary amine, the bond length of CO_2 becomes longer, the O—C—O bond of CO_2 begins to bend, HO—H of the H_2O bond breaks, amine and H_2O form an H—N bond, and CO_2 and OH begin to from a C—O bond. The OH formed by HO—H fracture forms a hydrogen bond with the H of the N—OH, which makes it more stable and conducive to the transfer of a proton H to N. It can be seen that the bond lengths of N—H in the transition states of DMA2P (Figure 4A) and DEA2P (Figure 4B) are 1.093 and 1.089 Å respectively, which are very close to the bond lengths of N—H in the final state of N-H bonding.

Subsequently, the intrinsic reaction coordinate (IRC) method was performed on the transition state. The initial and final states obtained from IRC were optimized. The free energy barrier diagram of DEA2P and DMA2P is shown in Figure 5. It can be seen from the figure that the DEA2P reaction free energy barrier is lower than the DMA2P reaction free energy barrier (8.04 kcal/mol < 9.83 kcal/mol). In addition, from the initial state (Figure 5 DEA2P(DMA2P) + H_2O + CO_2), we found that H_2O can exist stably in the lone pair direction of N because of the hydrogen-bond interaction. The IRI diagram on the left of Figure 5 proves that hydrogen-bond interactions exist between H_2O and the amine (the part circled in red). Therefore, we speculated that the initial structures of DMA2P and DEA2P would be more conducive to the adsorption of H_2O molecules for the protic reaction.

3.1.2 | Reaction mechanism and free energy barrier calculation of CO_2 absorption in aqueous secondary amine solutions

Based on the zwitterion mechanism, the reaction between CO_2 and secondary amines is a two-step reaction. The transition state in Equation (2) and the transition state in Equation (3) were denoted as TS1 and TS2, respectively. Their calculated structures are shown in Figure 6. As can be seen from TS1 in Figure 6, amines react directly with CO_2 to form zwitterion in the first step. Then, the zwitterions undergo proton transfer to another amine through an H_2O molecule, as shown in Figure 6C,D. In this study, we considered that it is difficult for the zwitterion to transfer protons to amines at lower concentrations. Therefore, when we calculate TS2, we let the zwitterion transfer the proton to the amine molecule with the help of H_2O. As can be seen from TS2 in Figure 6, at the beginning of the reaction, the O—H bond of H_2O was first broken and the H atom was attracted by the amine molecule. After that, the N—H bond was formed with the amine molecule, while the N—H bond of the zwitterion began to break, and the O—H bond of H_2O began to slowly form. At this time, the bond energy of zwitterion N—H determines the level of the free energy barrier. It can also be seen from Figure 15 and Table 5 that the formed N—H bond is stronger than the formed O—H bond. From the TS2 structure diagram of MAE^+COO^- (Figure 6C) and EAE^+COO^- (Figure 6D), we also find that the N—H bond lengths of MAE^+COO^- and EAE^+COO^- are 1.210 and 1.233 Å, respectively. Therefore, we speculate that MAE^+COO^- N—H bond is more likely to break and the free energy barrier should be lower for deprotonation of the zwitterion.

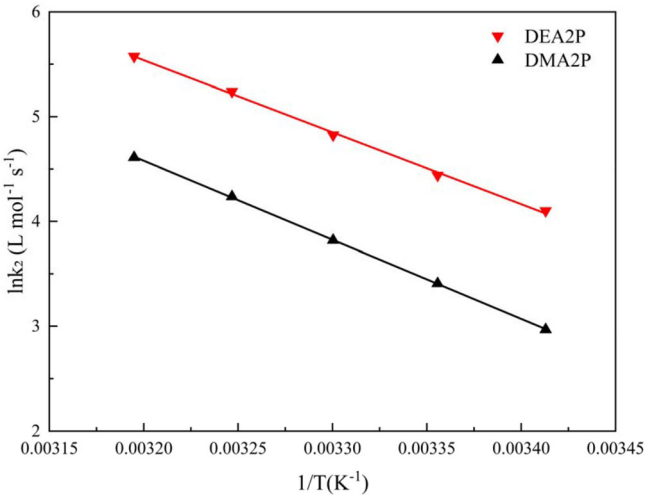

FIGURE 9 The Arrhenius plot of DEA2P and DMA2P.

The intrinsic reaction coordinate (IRC) analysis was then performed on both transition states, and free energy barriers of reactions in EAE and MAE solutions were obtained, as shown in Figure 7. It can be seen that the free energy barriers of MAE and EAE in part I are very low and close (2.25 and 1.56 kcal/mol), while the free energy barrier of MAE^+COO^- in part II was lower than that of EAE^+COO^- (4.01 < 5.38 kcal/mol). Meanwhile, we found that the free energy barrier of part II was higher than that of part I, so part II is the rate control step for this reaction process.

3.2 | Experimental results

3.2.1 | Kinetics of CO_2 absorption in aqueous tertiary amine solutions

The kinetics of CO_2 absorption by DEA2P and DMA2P were studied for the temperature range of 293–313 K and under the concentration of 0.1–0.2 kmol/m^3, and the measured k_0 is shown in

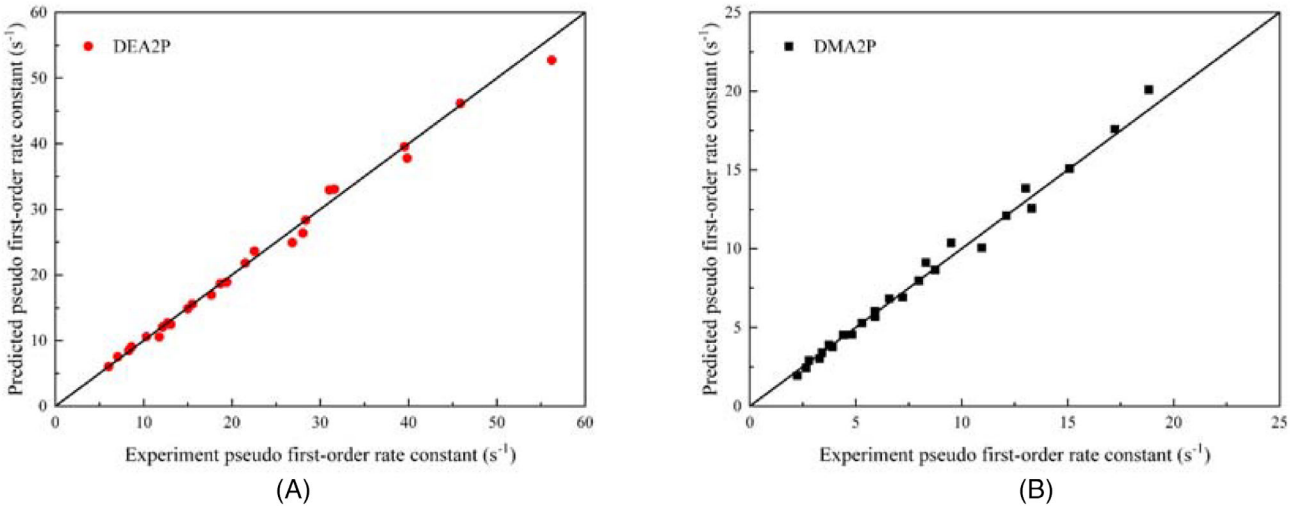

FIGURE 10 The relationship between the experimental k_0 and the predicted k_0 in aqueous DEA2P (A) and DMA2P (B) solutions.

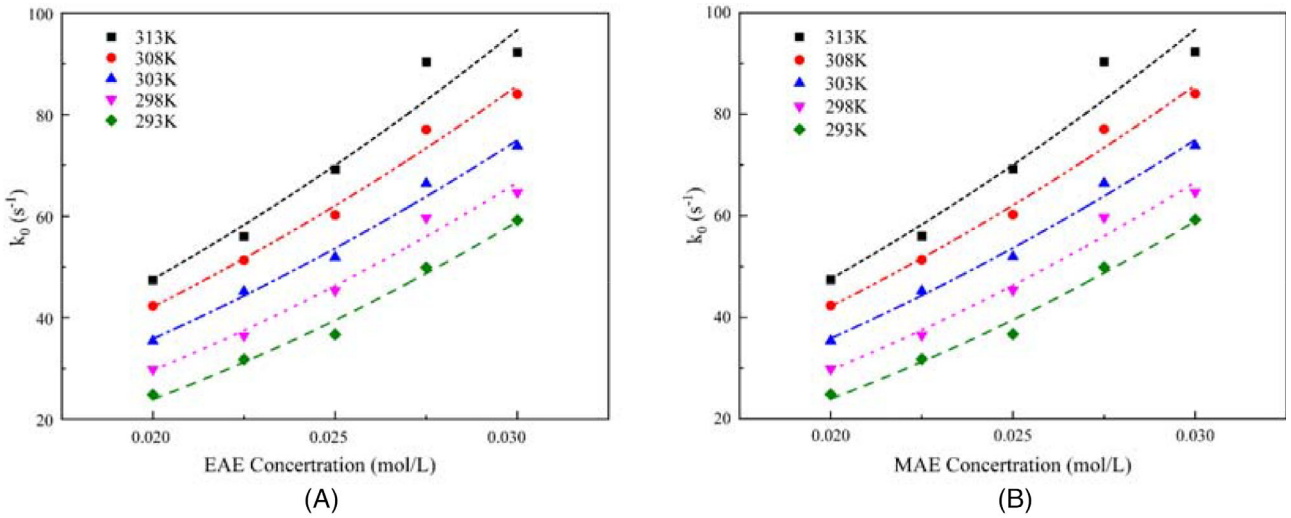

FIGURE 11 The k_0 of EAE (A) and MAE (B) as function of concentration at different temperatures.

TABLE 2 CO_2-EAE(MAE)-water system three-order reaction rate constants at different temperatures

	EAE		MAE	
Temperatures (K)	k_3^{EAE}	$k_3^{H_2O}$	k_3^{MAE}	$k_3^{H_2O}$
293	30,842 ± 377	0.32 ± 0.18	60,356 ± 1431	0.63 ± 0.72
298	37,243 ± 1126	0.36 ± 0.48	70,988 ± 1483	0.72 ± 0.71
303	44,000 ± 1411	0.41 ± 0.63	85,000 ± 1438	0.83 ± 0.71
308	52,697 ± 1585	0.46 ± 0.39	98,100 ± 2044	0.89 ± 1.00
313	62,426 ± 1984	0.51 ± 1.00	108,455 ± 3441	1.01 ± 1.62

Figure 8. It is easy to see that k_0 increases with increasing concentration and temperature. By fitting the k_0 values using the empirical power law relationship, the reaction orders can be obtained, all of which are very close to 1. The results indicate that the base-catalyzed hydration mechanism can be used to explain the reaction between CO_2 and DEA2P or DMA2P, which is identical to our calculation results. Then the second-order reaction rate constants (k_2) of DEA2P and DMA2P were calculated and are listed in Table 1, respectively.

The Arrhenius plot for k_2^{DEA2P} and k_2^{DMA2P} as a function of temperature ($1/T$) is shown in Figure 9. Thus, the Arrhenius equation of DEA2P and DMA2P can be expressed as:

$$k_2^{DEA2P} = 9.09 \times 10^{11} \exp\left(\frac{-6874.3}{T}\right) \quad (12)$$

$$k_2^{DMA2P} = 3.03 \times 10^{12} \exp\left(\frac{-7549.8}{T}\right) \quad (13)$$

Moreover, the activation energies (E_a) of DEA2P and DMA2P are calculated to be 13.66 and 15.00 kcal/mol, respectively, which is consistent with the calculated free energy barrier of DEA2P being smaller than DMA2P. So, the increase in chain length shows a positive effect on the kinetic reaction rate of CO_2 absorption by tertiary amines.

The comparison between the experimental values and predicted values of k_0 is shown in Figure 10. The predicted values of k_0 are in good agreement with experimental values, with acceptable average absolute relative deviations (AARD) for DEA2P and DMA2P being 3.28% and 4.47%, respectively. Combined with the previous simulation results, the base-catalyzed hydration mechanism can accurately describe the experimental results of CO_2 absorption by DEA2P and DMA2P.

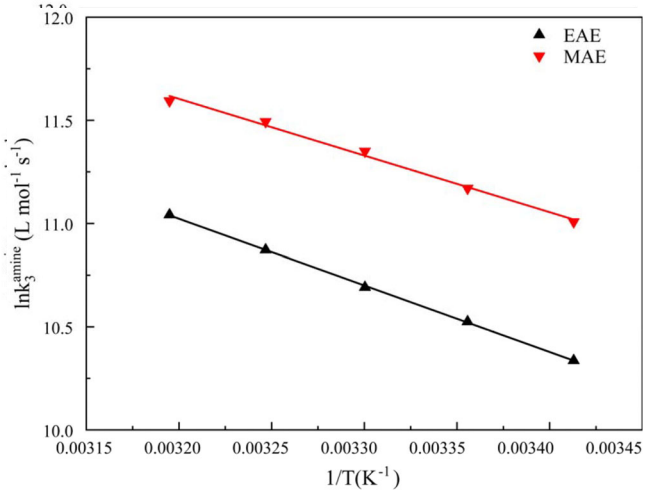

FIGURE 12 The Arrhenius plot of EAE and MAE.

3.2.2 | Kinetics of CO_2 absorption in aqueous secondary amine solutions

Based on the simulation results, the zwitterion mechanism with the rate-limiting step of deprotonation was selected for the kinetic model of EAE and MAE. Under the same operating conditions, under a temperature range of 293–313 K, the kinetics of CO_2 absorption by EAE and MAE were studied for the concentration range of 0.02–0.03 kmol/m^3. The change of k_0 measured with the concentration of EAE(MAE) under different temperatures is shown in Figure 11. By fitting k_0 values with empirical power law relations, all reaction orders are very close to 2. Then, the real third-order reaction rate constants of EAE and MAE (k_3) were calculated by the zwitterionic mechanism and listed in Table 2. We found that $k_3^{H_2O}$ is much smaller than k_3^{amine}, so we will not discuss the effects of H_2O receiving protons, which is consistent with the simulation where water does not accept the proton, but simply delivers the proton to the amine. The Arrhenius plot for k_3^{EAE} and k_3^{MAE} as functions of ($1/T$) is shown in Figure 12. Thus, the Arrhenius equation of EAE and MAE can be expressed as:

TABLE 3 $\Delta E_{strain}(TS)$ and $\Delta E_{int}(TS)$ of MAE(TS2), EAE(TS2), DMA2P, and DEA2P

E(kcal/mol)	MAE(TS2)	EAE(TS2)	DMA2P	DEA2P
$\Delta E_{strain}(TS)$	64.46	66.79	55.92	60.91
$\Delta E_{int}(TS)$	−60.45	−61.41	−46.09	−52.87
$\Delta E(TS)$	4.01	5.38	9.83	8.04

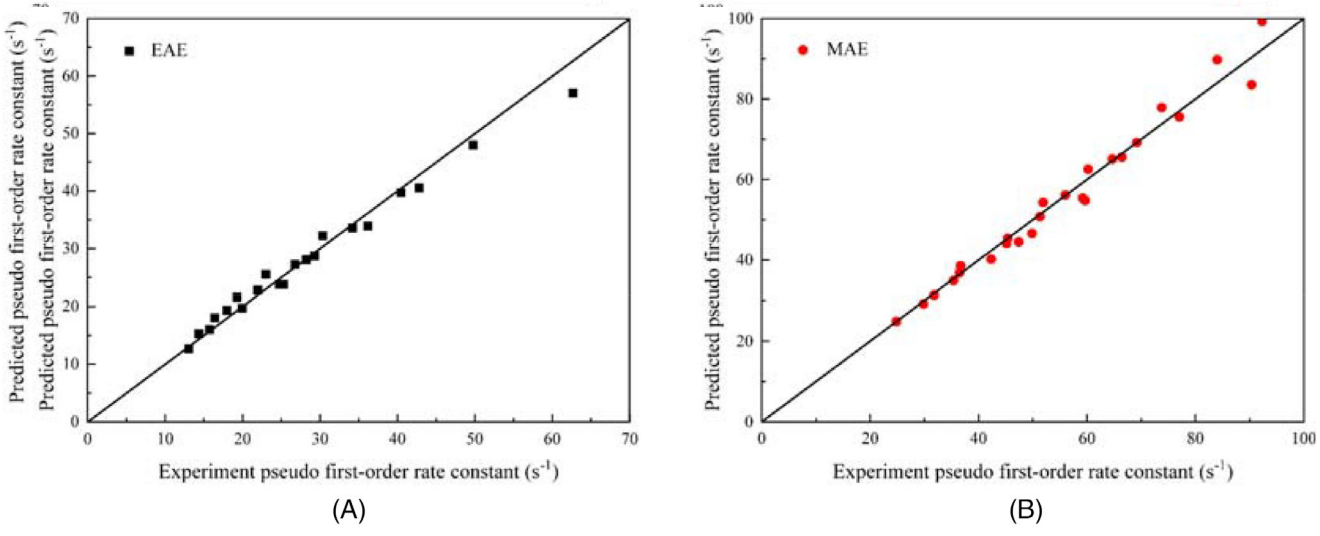

FIGURE 13 The relationship between the experimental k_0 and the predicted k_0 in aqueous EAE (A) and MAE (B) solutions.

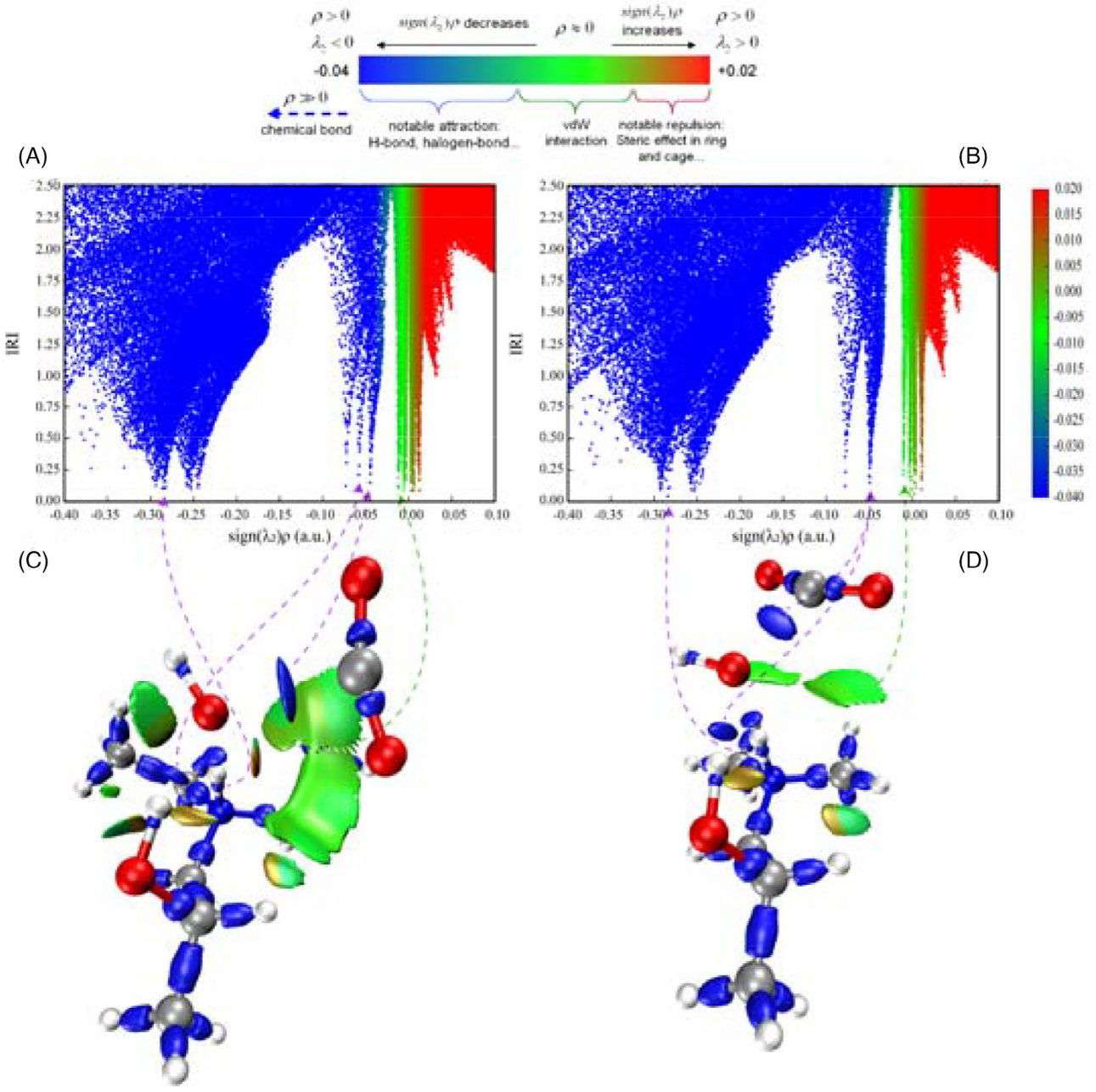

FIGURE 14 interaction region indicator (IRI): (A) IRI vs. Sign ($\lambda 2$)ρ scatter plot of DEA2P; (B) IRI vs. Sign ($\lambda 2$)ρ scatter plot of DMA2P; (C) chemical bonds and weak interactions diagram of DEA2P; (D) chemical bonds and weak interactions diagram of DMA2P. The dotted line corresponds to the interaction energy term and the corresponding size.

$$k_3^{\mathrm{EAE}} = 1.85 \times 10^9 \exp\left(\frac{-3223.2}{T}\right) \quad (14)$$

$$k_3^{\mathrm{MAE}} = 7.76 \times 10^8 \exp\left(\frac{-2747.4}{T}\right) \quad (15)$$

Moreover, the activation energies (E_a) of EAE and MAE were 6.40 and 5.46 kcal/mol, respectively, which is consistent with the TS2 calculated free energy barrier of MAE being smaller than EAE. Therefore, the increase in chain length has a negative effect on the kinetic reaction rate of secondary amine absorption of CO_2.

The experimental and predicted values of k_0 are shown in Figure 13. As shown there, the predicted values of k_0 are in good agreement with experimental values, and the average absolute relative deviations (AARD) of EAE and MAE were acceptable at 4.91% and 2.99%, respectively. Combined with the previous simulation results, the zwitterion mechanism accurately describes the experimental data of CO_2 absorption by EAE and MAE.

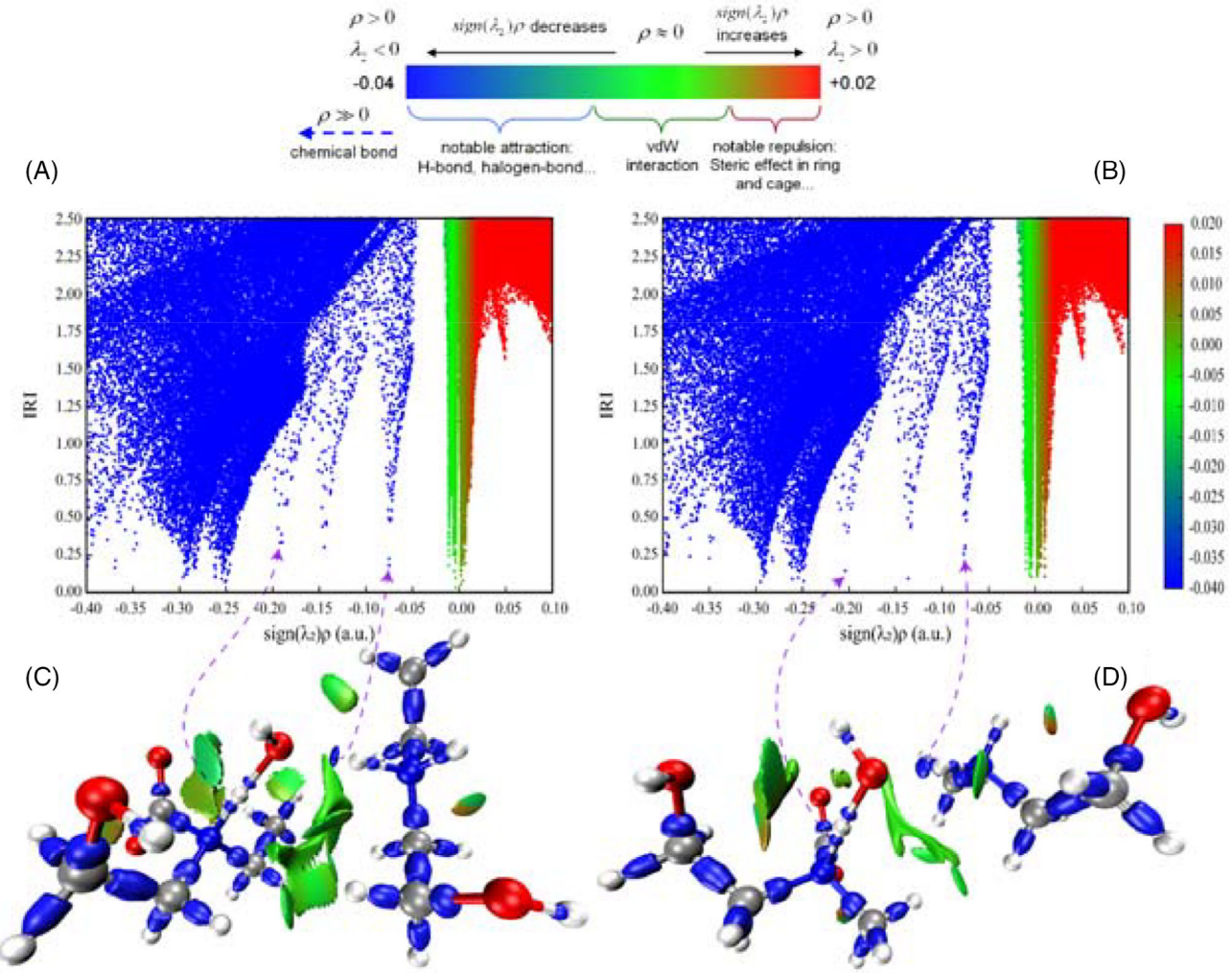

FIGURE 15 interaction region indicator (IRI): (A) IRI vs. Sign ($\lambda 2)\rho$ scatter plot of EAE; (B) IRI vs. Sign ($\lambda 2)\rho$ scatter plot of MAE; (C) chemical bonds and weak interactions diagram of EAE; (D) chemical bonds and weak interactions diagram of MAE. The dotted line corresponds to the strain energy term and the corresponding size.

3.3 | The effects of chain lengths on CO_2 absorption

The before-mentioned experimental and computational analyses show that for tertiary amines, the increase of chain length is beneficial to accelerating the CO_2 absorption rate while for secondary amines, the increase of chain length slows down the CO_2 absorption rate. In addition, the energy barrier of the zwitterion mechanism is lower than that of the base-catalyzed hydration mechanism, which is consistent with the experimental results, where, when the primary or secondary amine is close to the pKa of the tertiary amine, the primary or secondary amine reacts faster. The pKa of aqueous MAE, EAE, DMA2P, and DEA2P solutions are 9.88, 10.0, 9.67, and 9.92, respectively.[59–61]

To further explore the molecular mechanism, the activation strain model was used to analyze the energy barrier. By dividing the energy change $\Delta E(TS)$ of the transition state into the strain energy term ΔE_{strain} and the interaction energy term ΔE_{int}, namely:

$$\Delta E(TS) = \Delta E_{strain}(TS) + \Delta E_{int}(TS) \quad (16)$$

In this study, the strain energy term:

$$\Delta E_{strain}(TS) = E_1(TS) + E_2(TS) + E_3(TS) - E_{total}(IS) \quad (17)$$

the interaction energy term:

$$\Delta E_{int}(TS) = E_{total}(TS) - E_1(TS) - E_2(TS) - E_3(TS) \quad (18)$$

where $E_i(TS)$ (i=1, 2, 3) is the free energy of the transition state fragment (reactant) i, $E_{total}(IS)$ is the total free energy of the initial state, and $E_{total}(TS)$ is the total free energy of the transition state.

$\Delta E_{strain}(TS)$ and $\Delta E_{int}(TS)$ were then calculated and are listed in Table 3. For secondary amines, as the chain length increases, $\Delta E_{strain}(TS)$ increases, $\Delta E_{int}(TS)$ decreases, and $\Delta E_{strain}(TS)$ changes more. Therefore, the increase in the free energy barrier is mainly due

TABLE 4 ρ(BCP) and V(BCP) of the interaction bond critical points of two tertiary amines.

	DEA2P				DMA2P			
Interaction	N—H	H-bond	vdW	C—O	N—H	H-bond	vdW	C—O
ρ(BCP)	0.288	0.0582	0.0058	0.045	0.285	0.0506	0.0038	0.050
V(BCP)	−0.497	−0.0598	−0.0031	−0.0346	−0.492	−0.0495	−0.0020	−0.039

TABLE 5 ρ(BCP) and V(BCP) of the strain bond critical points of two secondary amines.

	EAE		MAE	
Strain	OOCN—H	HO—H	OOCN—H	HO—H
ρ(BCP)	0.192	0.0756	0.204	0.0765
V(BCP)	−0.261	−0.0802	−0.290	−0.0811

to the strain energy term which includes the breaking of the N-H bond of the zwitterion and the breaking of the O—H bond of the H_2O molecule.

Similarly, we found that for secondary amines, the increase in the free energy barrier is mainly due to the interaction energy term which includes the chemical bonds and interactions between amine and H_2O, amine and CO_2, and H_2O and CO_2.

To describe these chemical bonds and interactions more intuitively, the Interaction Region Indicator (IRI) analysis diagrams of tertiary and secondary amines were drawn in Figures 14 and 15, respectively. In addition, for tertiary amines, the electron density ρ(BCP), and the potential energy density V(BCP) of the interaction bond critical points in Table 4 were obtained by means of topological analysis in Atoms in Molecules (AIM) analysis. For the secondary amines, ρ(BCP) and V(BCP) of the strain bond critical points are shown in Table 5. For the same kind of chemical bonds, generally the larger the ρ(BCP), the more negative the V(BCP), the greater the chemical bond strength, the lower the bond energy, and the lower the molecular structure energy.

For the reaction process of tertiary amines (DMA2P and DEA2P), we can see that the chemical bonds and interactions which correspond to the interaction energy term of tertiary amines have the chemical bonds of N—H between amine and H_2O, C—O between H_2O and CO_2, the interaction of hydrogen bond between the hydroxyl of amine and H_2O and vdW interaction between amine and CO_2. It can also be seen from Table 4 that the chemical bond and interactions of DEA2P have lower energy for all bonds except the C—O bond because of the larger ρ(BCP) and the more negative V(BCP). In addition, the isosurface of the vdW interaction part of DEA2P is larger (Figure 14C,D corresponding area of green line). So, the free energy barrier of DEA2P is lower, which explains why the increase in chain length of the tertiary amines is conducive to the absorption of CO_2.

Meanwhile the chemical bonds corresponding to the strain energy term of the secondary amine can be seen in Figure 15C,D. It can also be seen from Table 5 that for MAE(TS2), the ρ(BCP) of the N—H and HO—H bonds are larger and the V(BCP) of these are more negative than EAE(TS2). So, the N—H and HO—H bonds of MAE(TS2) have the lower energy, which make the free energy barrier lower. This explains why the increase in chain length of the secondary amines is not conducive to deprotonation reactions and thus to the absorption of CO_2.

As can be seen from the discussion above, the increase in the chain length of amine molecules makes its attraction to protons increase. For tertiary amines, the longer chain length causes the amines to more strongly attract protons, and makes the hydrogen-bond interaction with H_2O and the vdW attraction to CO_2 stronger in the transition state of their base-catalyzed hydration reactions, thereby reducing the free energy barrier. For secondary amines, the increase in chain length increases the energy of the N—H bond in the zwitterion and the HO—H bond of H_2O in the transition state of the proton transfer reaction, thus increasing the free energy barrier.

4 | CONCLUSIONS

In this study, the reaction mechanism of CO_2 absorption in secondary and tertiary amine solutions and the effect of chain length on reaction kinetics were explored by combined DFT calculation and stopped-flow kinetic analysis. Based on the simulation results, the base-catalyzed hydration mechanism for tertiary amines and the zwitterion mechanism with the rate-limiting step of zwitterion deprotonation for secondary amines were confirmed. Then, this reaction mechanism was used to fit experimental data, showing great predictive potential. At the same time, the free energy barriers of the reactions and the activation energy barriers of the reactions were also obtained. The free energy barrier obtained by DFT is consistent with the activation energy barrier trend obtained by experiment. Combining the calculated free energy barrier with the experimental activation energy barrier, it was found that the increase in chain length has a positive effect on the kinetic reaction rate of tertiary amines to absorb CO_2, while for secondary amines, the opposite is the case.

Additionally, the energy barrier of the zwitterion mechanism is lower than that of the base-catalyzed hydration mechanism, which is consistent with the experimental results, where, when the primary or secondary amine is close to the pKa of the tertiary amine, the primary or secondary amine reacts faster. Then, the activation strain model with the Interaction Region Indicator (IRI) method and Atoms in Molecules (AIM) analysis were combined to essentially explain the level of the free energy barrier. It was found that the increase in tertiary amines chain length has a positive effect on the interaction of the reactants, resulting in the reduction of the energy barrier. For

secondary amines, the chain length increase has a negative effect on the strain of the reactants, resulting in the increased energy barrier.

AUTHOR CONTRIBUTIONS

Ding Wei: Data curation (lead); formal analysis (lead); methodology (lead); software (lead); writing – original draft (lead). **Qinlan Luo:** Investigation (lead); software (supporting); writing – review and editing (supporting). **Tong Ouyang:** Visualization (lead). **Qie Liu:** Data curation (supporting). **Yangqiang Huang:** Investigation (supporting). **Bo Jin:** Visualization (supporting). **Hongxia Gao:** Funding acquisition (supporting). **Xiao Luo:** Conceptualization (equal); supervision (lead); writing – review and editing (supporting). **Zhiwu Liang:** Project administration (lead); resources (lead).

ACKNOWLEDGMENT

This work was supported by the National Natural Science Foundation of China (NSFC Nos. 22178089). The authors especially thank Wilfred Olson and Yu Mao for their revisions of the article. Computational Chemistry Commune for its answers to theoretical computational questions and Shiyi Wei and Jigang Du for helping with experiments are also gratefully acknowledged.

DATA AVAILABILITY STATEMENT

The data that support the findings of this study are available from the corresponding author upon reasonable request.

ORCID

Xiao Luo https://orcid.org/0000-0003-2201-7586
Zhiwu Liang https://orcid.org/0000-0003-1935-0759

REFERENCES

1. Yamasaki A. An overview of CO_2 mitigation options for global warming-emphasizing CO_2 sequestration options. *J Chem Eng JPN*. 2003;36:361-375.
2. Kätelhön A, Meys R, Deutz S, Suh S, Bardow A. Climate change mitigation potential of carbon capture and utilization in the chemical industry. *Proc Natl Acad Sci*. 2019;116(23):11187-11194.
3. Bui M, Adjiman CS, Bardow A, et al. Carbon capture and storage (CCS): the way forward. *Energ Environ Sci*. 2018;11(5):1062-1176.
4. Qinlan L, Feng B, Zhuhan L, Zhou Q, Zhang Y, Li N. Experimental study on simultaneous absorption and desorption of CO_2/SO_2/NO_x using aqueous MDEA + DMSO solutions. *Energy Fuel*. 2018;32(3):3647-3659.
5. Yang X, Rees RJ, Conway W, Puxty G, Yang Q, Winkler DA. Computational modeling and simulation of CO_2 capture by aqueous amines. *Chem Rev*. 2017;117(14):9524-9593.
6. Dutcher B, Fan M, Russell AG. Amine-based CO_2 capture technology development from the beginning of 2013—a review. *ACS Appl Mater Interfaces*. 2015;7(4):2137-2148.
7. Rochelle GT. Amine scrubbing for CO_2 capture. *Science*. 2009;325(5948):1652-1654.
8. Campbell M. Technology innovation & advancements for shell cansolv CO_2 capture solvents. *Energy Procedia*. 2014;63:801-807.
9. Singh A, Stéphenne K. Shell Cansolv CO_2 capture technology: achievement from first commercial plant. *Energy Procedia*. 2014;63:1678-1685.
10. Li W, Wen S, Shen L, Zhang Y, Sun C, Li S. Mechanism and kinetic study of carbon dioxide absorption into a methyldiethanolamine/1-hydroxyethyl-3-methylimidazolium lysine/water system. *Energy Fuel*. 2018;32(10):10813-10821.
11. MacDowell N, Florin N, Buchard A, et al. An overview of CO_2 capture technologies. *Energ Environ Sci*. 2010;3(11):1645-1669.
12. Conway W, Wang X, Fernandes D, et al. Toward the understanding of chemical absorption processes for post-combustion capture of carbon dioxide: electronic and steric considerations from the kinetics of reactions of CO_2(aq) with sterically hindered amines. *Environ Sci Technol*. 2013;47(2):1163-1169.
13. Mumford KA, Wu Y, Smith KH, Stevens GW. Review of solvent based carbon-dioxide capture technologies. *Front Chem Sci Eng*. 2015;9(2):125-141.
14. Oh S-Y, Binns M, Cho H, Kim J-K. Energy minimization of MEA-based CO_2 capture process. *Appl Energy*. 2016;169:353-362.
15. Zheng W, Luo Q, Liu S, et al. New method of kinetic modeling for CO_2 absorption into blended amine systems: a case of MEA/EAE/3-DEA1P trisolvent blends. *AIChE J*. 2022;68(6):e17628.
16. Versteeg GF, van Swaaij WPM. On the kinetics between CO_2 and alkanolamines both in aqueous and non-aqueous solutions—I. Primary and secondary amines. *Chem Eng Sci*. 1988;43(3):573-585.
17. Conway W, Wang X, Fernandes D, et al. Toward rational design of amine solutions for PCC applications: the kinetics of the reaction of CO_2 (aq) with cyclic and secondary amines in aqueous solution. *Environ Sci Technol*. 2012;46(13):7422-7429.
18. Rayer A, Henni A. Heat of absorption of CO_2 in aqueous solutions of tertiary amines: N-methyl diethanolamine (MDEA), 3-dimethylamino-1-propanol (3DMAP), and 1-dimethylamino-2-propanol (1DMAP). *Ind Eng Chem Res*. 2014;53(12):4953-4965.
19. Xiao M, Liu H, Idem R, Tontiwachwuthikul P, Liang Z. A study of structure–activity relationships of commercial tertiary amines for post-combustion CO_2 capture. *Appl Energy*. 2016;184:219-229.
20. Kadiwala S, Rayer AV, Henni A. Kinetics of carbon dioxide (CO_2) with ethylenediamine, 3-amino-1-propanol in methanol and ethanol, and with 1-dimethylamino-2-propanol and 3-dimethylamino-1-propanol in water using stopped-flow technique. *Chem Eng J*. 2012;179:262-271.
21. Shen S, Yang Y-N, Bian Y, Zhao Y. Kinetics of CO_2 absorption into aqueous basic amino acid salt: potassium salt of lysine solution. *Environ Sci Technol*. 2016;50(4):2054-2063.
22. N.Borhani T, Wang M. Role of solvents in CO_2 capture processes: the review of selection and design methods. *Renew Sustain Energy Rev*. 2019;114:109299.
23. Hwang SJ, Kim J, Kim H, Lee KS. Solubility of carbon dioxide in aqueous solutions of three secondary amines: 2-(Butylamino)ethanol, 2-(Isopropylamino)ethanol, and 2-(Ethylamino)ethanol secondary Alkanolamine solutions. *J Chem Eng Data*. 2017;62(8):2428-2435.
24. Shi X, Li C, Guo H, Shen S. Density, viscosity, and excess properties of binary mixtures of 2-(methylamino)ethanol with 2-methoxyethanol, 2-ethoxyethanol, and 2-butoxyethanol from 293.15 to 353.15 K. *J Chem Eng Data*. 2019;64(9):3960-3970.
25. Yu C-H, Huang C-H, Tan C-S. A review of CO_2 capture by absorption and adsorption. *Aerosol Air Qual Res*. 2012;12(5):745-769.
26. Zhang R, Yang Q, Liang Z, et al. Toward efficient CO_2 capture solvent design by analyzing the effect of chain lengths and amino types to the absorption capacity, bicarbonate/carbamate, and cyclic capacity. *Energy Fuel*. 2017;31(10):11099-11108.
27. Jiang W, Xe H, Luo X, et al. A comparative kinetics study of CO_2 absorption into aqueous DEEA/MEA and DMEA/MEA blended solutions. *AIChE J*. 2018;64(4):1350-1358.
28. Wolters LP, Bickelhaupt FM. The activation strain model and molecular orbital theory. *Wiley Interdiscip Rev Comput Mol Sci*. 2015;5(4):324-343.
29. Bickelhaupt FM, Houk KN. Analyzing reaction rates with the distortion/interaction-activation strain model. *Angew Chem Int Ed*. 2017;56(34):10070-10086.
30. Bader RFW, Beddall PM. Virial field relationship for molecular charge distributions and the spatial partitioning of molecular properties. *J Chem Phys*. 1972;56:3320-3329.

31. Bader RFW, Carroll MT, Cheeseman JR, Chang C. Properties of atoms in molecules: atomic volumes. *J Am Chem Soc*. 1987;109(26):7968-7979.
32. Astakhov AA, Tsirelson VG. Spatial localization of electron pairs in molecules using the fisher information density. *Chem Phys*. 2014;435:49-56.
33. Lipkowski P, Grabowski SJ, Robinson TL, Leszczynski J. Properties of the C− H...H dihydrogen bond: an ab initio and topological analysis. *J Phys Chem A*. 2004;108(49):10865-10872.
34. Liang Y, Liu H, Rongwong W, Liang Z, Idem R, Tontiwachwuthikul P. Solubility, absorption heat and mass transfer studies of CO_2 absorption into aqueous solution of 1-dimethylamino-2-propanol. *Fuel*. 2015;144:121-129.
35. Knipe AC, McLean D, Tranter RL. A fast response conductivity amplifier for chemical kinetics. *J Phys E: Sci Instr*. 1974;7(7):586-590.
36. Li J, Liu H, Liang Z, et al. Experimental study of the kinetics of the homogenous reaction of CO_2 into a novel aqueous 3-diethylamino-1,2-propanediol solution using the stopped-flow technique. *Chem Eng J*. 2015;270:485-495.
37. Li J, Henni A, Tontiwachwuthikul P. Reaction kinetics of CO_2 in aqueous ethylenediamine, ethyl ethanolamine, and diethyl monoethanolamine solutions in the temperature range of 298−313 K, using the stopped-flow technique. *Ind Eng Chem Res*. 2007;46(13):4426-4434.
38. Alper E, Bouhamra W. Reaction kinetics of carbonyl sulfide with aqueous ethylenediamine and diethylenetriamine. *Gas Sep Purif*. 1994;8(4):237-240.
39. Alper E. Kinetics of reactions of carbon dioxide with diglycolamine and morpholine. *Chem Eng J*. 1990;44(2):107-111.
40. Donaldson TL, Nguyen YN. Carbon dioxide reaction kinetics and transport in aqueous amine membranes. *Ind Eng Chem Fundam*. 1980;19(3):260-266.
41. Jensen MB, Jorgensen E, Faurholt C. Reactions between carbon dioxide and amino alcohols. 1. Monoethanolamine and diethanolamine. *Acta Chem Scand*. 1954;8(7):1137-1140.
42. Caplow M. Kinetics of carbamate formation and breakdown. *J Am Chem Soc*. 1968;90(24):6795-6803.
43. Gaussian 16 Rev. C.01 [computer program]. 2016.
44. Sholl DS, Steckel JA. *Density Functional Theory: A Practical Introduction*. John Wiley & Sons, Inc; 2009.
45. Molclus program. Version 1.9.9.9 [computer program]. http://www.keinsci.com/research/molclus.html.
46. Stephens PJ, Devlin FJ, Chabalowski CF, Frisch MJ. Ab initio calculation of vibrational absorption and circular dichroism spectra using density functional force fields. *J Phys Chem*. 1994;98(45):11623-11627.
47. Ditchfield R, Hehre WJ, Pople JA. Self-consistent molecular-orbital methods. IX. An extended Gaussian-type basis for molecular-orbital studies of organic molecules. *J Chem Phys*. 1971;54(2):724-728.
48. Feller D. The role of databases in support of computational chemistry calculations. *J Comput Chem*. 1996;17(13):1571-1586.
49. Pritchard BP, Altarawy D, Didier B, Gibson TD, Windus TL. New basis set exchange: an open, up-to-date resource for the molecular sciences community. *J Chem Inf Model*. 2019;59(11):4814-4820.
50. Schuchardt KL, Didier BT, Elsethagen T, et al. Basis set exchange: a community database for computational sciences. *J Chem Inf Model*. 2007;47(3):1045-1052.
51. Grimme S, Antony J, Ehrlich S, Krieg H. A consistent and accurate ab initio parametrization of density functional dispersion correction (DFT-D) for the 94 elements H-Pu. *J Chem Phys*. 2010;132(15):154104.
52. Cossi M, Rega N, Scalmani G, Barone V. Energies, structures, and electronic properties of molecules in solution with the C-PCM solvation model. *J Comput Chem*. 2003;24(6):669-681.
53. Weigend F, Ahlrichs R. Balanced basis sets of split valence, triple zeta valence and quadruple zeta valence quality for H to Rn: design and assessment of accuracy. *Phys Chem Chem Phys*. 2005;7(18):3297-3305.
54. Fukui K. The path of chemical reactions—the IRC approach. *Acc Chem Res*. 1981;14(12):363-368.
55. Lu T, Chen F. Multiwfn: a multifunctional wavefunction analyzer. *J Comput Chem*. 2012;33(5):580-592.
56. Humphrey W, Dalke A, Schulten K. VMD: visual molecular dynamics. *J Mol Graph*. 1996;14(1):33-38.
57. Lu T, Chen Q. Interaction region indicator: a simple real space function clearly revealing both chemical bonds and weak interactions. *Chem-Methods*. 2021;1(5):231-239.
58. Weinhold F. Natural bond critical point analysis: quantitative relationships between natural bond orbital-based and QTAIM-based topological descriptors of chemical bonding. *J Comput Chem*. 2012;33(30):2440-2449.
59. Gangarapu S, Marcelis AT, Zuilhof H. Accurate pKa calculation of the conjugate acids of alkanolamines, alkaloids and nucleotide bases by quantum chemical methods. *Chemphyschem*. 2013;14(5):990-995.
60. Liu H, Xiao M, Liang Z, Tontiwachwuthikul P. The analysis of solubility, absorption kinetics of CO_2 absorption into aqueous 1-diethylamino-2-propanol solution. *AIChE J*. 2017;63(7):2694-2704.
61. Chowdhury FA, Yamada H, Higashii T, Goto K, Onoda M. CO_2 capture by tertiary amine absorbents: a performance comparison study. *Ind Eng Chem Res*. 2013;52(24):8323-8331.

How to cite this article: Wei D, Luo Q, Ouyang T, et al. An experimental and theoretical study on the effects of amine chain length on CO_2 absorption performance. *AIChE J*. 2023; 69(4):e17960. doi:10.1002/aic.17960